The (in)fluence of light

Chris Bueley

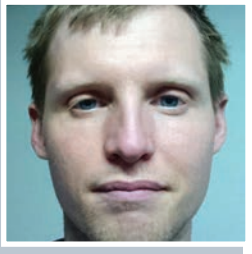

Dustin Olender

Bryce Bocking

Bueley, Olender, and Bocking describe how a technology that is widely used for disinfecting water, sterilizing surfaces, and destroying harmful microorganisms in food products and in air can also be used to inhibit unwanted marine growth on ocean sensors and other subsea equipment.

Who should read this paper?

This paper will be informative for anyone with an interest in in-situ ocean monitoring and those with an interest in alternate applications for LED technology.

Why is it important?

In the ocean environment, the term "biofouling" is used to describe unwanted growth of marine organisms on submerged equipment, including ocean sensors. It is widely recognized that biofouling is the primary factor limiting the useful life of ocean sensors that are deployed to monitor ocean conditions over extended periods of time (on the order of months to years). In some instances, sensors may be overrun with marine growth in less than a week. This paper presents a novel method of inhibiting marine growth: UV-C irradiation. The method is attractive in that it is non-contact, non-chemical, and suitable for a range of sensor materials and geometries. As such, it promises to be much more universally applicable than current strategies in that it may be equally suitable for chemical sensors, optical sensors, acoustic instruments, underwater lighting, etc. This method promises to dramatically increase the duration of deployment of ocean sensors, thereby reducing costs and improving data fidelity. The one drawback of the current UV-C antifouling technology is the relatively high power requirement (as much as 80 mA) which may be excessive for some power-sensitive deployments such as battery powered buoys. The technology is now commercially available for a variety of subsea applications.

About the authors

Chris Bueley has an M.A.Sc. in Mechanical Engineering from the University of Victoria (UVic) and has a background in the research and development of novel fibre-optic based sensors. He currently works for AML Oceanographic Ltd. where he is responsible for the development of new products. Dustin Olender is the Director of Engineering for AML Oceanographic Ltd. Prior to this he spent many years in product development at AML. He has a PhD in Mechanical Engineering from UVic where he focused on the design of a novel piezo-electric sensor. Bryce Bocking completed his B.Eng. with the UVic Mechanical Engineering department in 2014. As a student he worked with AML Oceanographic. He has also worked as a co-op student with NEPTUNE Canada and as a research assistant with the Institute for Integrated Energy Systems at the University of Victoria. Mr. Bocking is now working towards a M.A.Sc. with the West Coast Wave Initiative at UVic. His research involves modelling hydrodynamic forces of wave energy converters and visualizing breaking waves in a wave flume.

IN-SITU TRIAL OF UV-C AS AN ANTIFOULANT TO REDUCE BIOFOULING INDUCED MEASUREMENT ERROR

Chris Bueley, Dustin Olender, Bryce Bocking
AML Oceanographic, Sidney, BC, Canada

ABSTRACT

This work describes an investigation whereby UV-C radiation is trialled as a marine antifoulant to preserve measurement integrity of time-of-flight sound velocity sensors, optical turbidity sensors, and conductivity sensors in a nine-month in-situ deployment on an underwater observatory. UV radiation was emitted from a modular LED-based UV system embedded within the sensor cluster of the deployed instruments, with LED modules individually oriented to illuminate the various adjacent sensing structures of the protected sensors. A numerical model was developed and validated to estimate UV fluence in seawater. It was found that UV-C radiation was effective in preserving the measurement integrity of the sensors as well as inhibiting marine growth on adjacent structures. This work demonstrates the potential suitability of UV-C radiation to provide biofouling protection to a range of marine equipment including cameras, lights, ADCPs, etc., in addition to ocean sensors.

KEYWORDS

Biofouling; UV-C; Ultraviolet; Antifouling; UV LED; Biofilm

INTRODUCTION

Due to growing concern around global warming and other environmental impacts resulting from human activities, there is an increasing demand for monitoring of the world's oceans. Systems used to this effect typically consist of in-situ deployments of sensors and other monitoring equipment installed on a wide range of platforms including buoys, piers, autonomous vessels, and underwater observatories. These monitoring systems are usually autonomous and expected to provide reliable measurement data for many months to years. It is generally acknowledged that the principle factor limiting the duration of deployments is the unwanted growth of marine organisms on submerged equipment [Cooksey and Wigglesworth-Cooksey, 1995], referred to as biofouling [ACT, 2003]. Unchecked, this marine growth will inundate sensors, cameras, connectors, lights, and other equipment in days to weeks, well short of the required months to years. In extreme cases, sensor measurement integrity, generally the most important metric of a successful deployment, may become compromised in a matter of days. Cleaning fouled sensors while they are deployed is costly, if even possible. For this reason, much effort has been put forth over the years to develop biofouling mitigation strategies. These technologies can be generally categorized into three groups: 1) volumetric chemical dosing techniques, 2) surface coatings and treatments, and 3) mechanical methods.

The first strategy is characterized by the introduction of chemical antifoulants into the water in the vicinity of the protected surfaces, killing colonizing organisms. These chemical antifoulants may be synthesized in-situ, such as through electro-chlorination systems, or may be stored in the device prior to deployment. While these methods are considered the most effective [ACT, 2003], they are not preferred due to their harmful effects on the environment. Some chemical antifoulants such as TBT are banned in many jurisdictions due to environmental concerns. These methods are also limited in their application. Volumetric chemical dosing is most effective in scenarios where the volume of treated water is controlled, such as within a closed sensing chamber. In instances where no effort is made to control the flow of seawater to a sensor or structure, referred to as open-flow, the efficacy of the techniques diminishes due to the practicalities of controlling dose. This generally precludes their use for protecting cameras, ADCPs, lights, external field and inductive conductivity sensors, and other common open-flow equipment.

The second group of strategies are surface treatments, characterized as either chemical-leaching or non-stick coatings. Chemical-leaching methods work to kill colonizing organisms in contact with the treated surface. This includes copper tape and poison-leaching paints. Conversely, non-stick coatings are designed to limit surface adhesion thereby preventing fouling organisms from taking hold. In general, surface treatments are best suited for non-sensing surfaces such as instrument bodies and camera housings, and are not suitable for sensing structures (optical faces, electrodes, etc.) due to interference. For example, many optical sensors will not function correctly if the sensing faces are

coated, and some conductivity sensors are sensitive to the introduction of metal (i.e., copper tape) within their sensing volumes. A further limitation of non-stick coatings is that they require shear forces to self-clean. Sufficient shear forces are unlikely to be present on a stationary platform, necessitating periodic cleaning.

The third group of strategies is comprised of brushes and wipers utilized to mechanically remove fouling organisms. Criticisms of these strategies include poor reliability of the mechanical components and the tendency for the brushes themselves to become fouled. These methods are also not suitable for complex geometry; conductivity sensors, for example, cannot be easily brushed.

In recent years there have been encouraging reports on the use of ultraviolet radiation (UV) as an antifoulant [Cooksey and Wigglesworth-Cooksey, 1995; ACT, 2003; Lakretz et al., 2010; Delauney et al., 2010; Rand et al., 2007; Kolappan and Satheesh, 2011; Patil et al., 2007; Marconnet et al., 2011]. This strategy is attractive as it is non-contact, non-chemical, and suitable for complex geometries. UV-C radiation, defined as radiation with a wavelength between 200 and 280 nm, is currently employed for germicidal and disinfection purposes in the medical, industrial, and food industries. While its performance as a disinfectant is well characterized [EPA, 2003], there remains much to be learned about its use as a marine antifoulant. Patil et al. [2007] describe a study whereby the efficacy of UV-C radiation as a potential antifoulant for optical sensors is investigated by irradiating in-situ glass coupons with various intensities and exposure times. The study found UV-C to be effective at retarding biofilm development on the glass and thus a potential tool for protection of optical sensors. More recently, Lakretz et al. [2010] investigated water pre-treatment methods with various doses and wavelengths of UV, establishing that biofilm prevention is a function of UV wavelength, spectrum and dose (fluence). These results have been substantiated by others [Kolappan and Satheesh, 2011]. Additionally, Marconnet et al. [2011] have investigated the use of UV to maintain the integrity of nanofiltration (NF) membranes, concluding that UV pre-treatment of water is effective at reducing the deposition of biofouling materials on NF membranes. This also confirms a similar investigation done by others [Munshi et al., 2005].

While these initial investigations have shown promise, work to date has been limited to either irradiating non-functional surfaces (such as glass coupons) or applying a continuous pre-treatment method to a controlled water volume. It is not apparent how these results extend to protection of in-situ ocean sensors from biofouling induced measurement error because 1) many sensors have sensing structures more complex than glass windows, 2) many sensors and other equipment are deployed "open-flow" thereby precluding the use of water pre-treatment strategies, and 3) the sensors are subject to near-continuous adsorption of colonizing organisms. Performance metrics have similarly been limited to either assessing the prevention of biofilm development or the inactivation of colonizing (or pathogenic) organisms, as opposed to maintaining functionality of a sensor. To the knowledge of the authors, there

is no described work which extends these initial results to the preservation of measurement integrity for sensors in open-flow, long term, in-situ deployments. This knowledge is required to assess the suitability of UV radiation as an antifoulant for ocean monitoring purposes.

Described here is a long-term in-situ trial whereby UV-C is utilized to inhibit marine growth on ocean monitoring sensors deployed on an underwater observatory. The objective of this investigation was to evaluate the suitability of a UV-based antifoulant to prevent biofouling-induced measurement error in various ocean sensors; specifically regarding optical turbidity sensors, time-of-flight sound velocity sensors, and conductivity sensors. Performance was assessed both by visual inspection of the sensors and by quantifying measurement integrity over the nine-month deployment. Consideration was also given to the technique's ability to retard fouling on adjacent structures and equipment. This paper begins with a brief discussion of the operating principle of UV as an antifoulant then proceeds to describe the materials and methods of the investigation, including development and validation of a light model to estimate UV fluence. Experimental results are then detailed and followed by a discussion.

UV Light as an Antifoulant

The progression of biofouling is generally considered to occur in five stages, summarized by Delauney et al. [2010]. The first stage is characterized by the adsorption of both organic and inorganic molecules on a surface immediately following immersion, forming the basis of the primary film. In the second stage, microbial cells and bacteria are transported and fixed to the filmed surface. In the third stage, bacteria begin production of an extracellular polymer network, forming a microbial film. The fourth stage of biofouling sees the development of increasingly complex communities consisting of multicellular organisms, microalgae, debris, sediments, etc. Attachment of higher order organisms such as barnacles and mussels occur in the fifth and final stage of development.

Many these stages are characterized by the development of bacterial and cellular networks, referred to as biofilms, which form the groundwork for higher order communities. At a fundamental level, the primary mechanism for development of these biofilms is cellular reproduction of colonizing cells. It is through disruption of this cellular reproduction that ultraviolet radiation acts as an antifoulant. Much of the ultraviolet radiation present in the UV-C band is absorbed by DNA nucleotides [EPA, 2003]. Absorption of this radiation leads to the destruction of cellular DNA which results in the prevention of cellular reproduction, referred to as inactivation, and if the dosage is sufficient, cellular death [Hijnen et al., 2006]. By preventing adsorbing cells from dividing (or by killing them), UV irradiation inhibits the development of organic films and early-stage colonizers, which in turn prevents the development of higher order communities.

MATERIALS AND METHODS

Three customized instruments (Metrec•X, AML Oceanographic, Sidney, BC) were deployed to an ocean observatory operated by

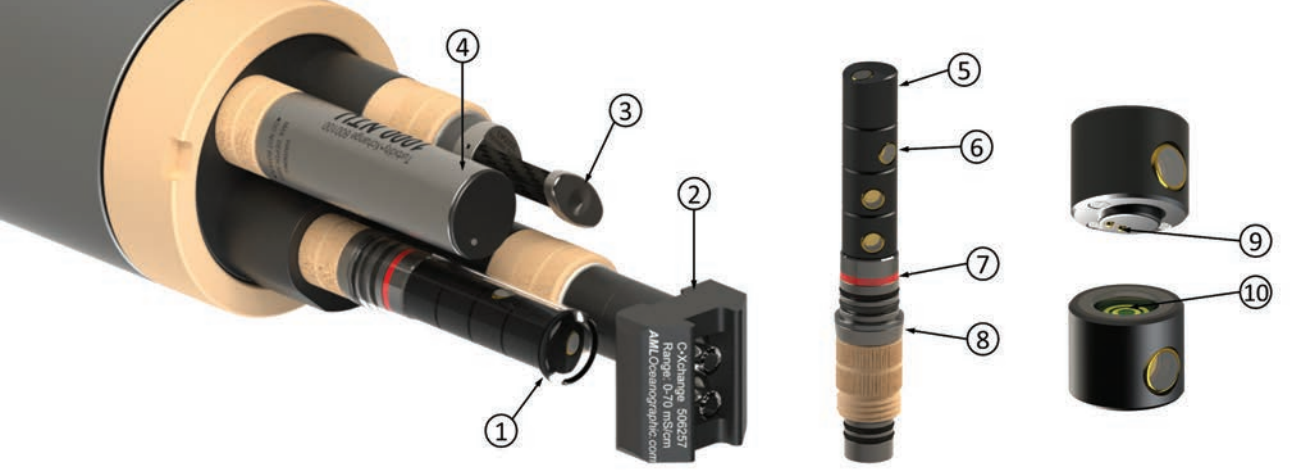

Figure 1: UV system mechanical embodiment. (1) protective quartz tube, (2) conductivity sensor, (3) time-of-flight sound velocity sensor, (4) turbidity sensor, (5) upwards-facing LED model, (6) sideways-facing LED module, (7) UV emission indicator ring, (8) titanium stem, (9) spring contact pins, (10) ring contact PCB.

Ocean Networks Canada (ONC). The observatory was located on the Folger Pinnacle off the coast of Vancouver Island, Canada, at a depth of 20 m. The location was known to have aggressive seasonal fouling due to its shallow depth and nutrient-rich waters. Two of the deployed instruments, referred to as UV1 and UV2, were equipped with purpose-built UV emission systems (described in the next section) and one was left unprotected as a control. Common to all instruments was an external field electrical conductivity sensor (XCH-CND-RA070, AML Oceanographic, BC), a time-of-flight sound velocity sensor (XCH-SV-STD, AML Oceanographic, BC), and an optical turbidity sensor (XCH-TRB-1000-05, AML Oceanographic, BC). The control instrument was also equipped with a pressure sensor (XCH-PRX-0100, AML Oceanographic, BC). The three instruments were secured with a custom-built mounting bracket that fixed the instruments horizontally and immediately adjacent to one another. PVC plates were installed between each instrument to prevent UV "spillover" from one instrument to the next.

Also deployed on the observatory platform was a reference instrument to provide comparative conductivity readings (Sea-Bird SeaCAT, SBE19plus, Sea-Bird, Bellevue, WA). The internal field conductivity sensor of the reference instrument was protected from biofouling with a chemical-based pumped antifouling system, considered the current industry gold standard. A controllable high definition camera (SNC-RH124, Sony, Japan) was also installed on the platform which provided real-time footage via web interface. The camera was programmed to record footage of the three test instruments daily at 17:00 UTC to visually monitor fouling.

All instruments were deployed to the platform on October 24, 2013, and retrieved for servicing on July 22, 2014. Data was collected from each sensor at a scan rate of 1 Hz and logged via ONC's logging software.

Mechanical Embodiment of UV system

UV emission was facilitated via a series of cylindrical, stackable modules housed within a protective quartz tube, as shown in Figure 1. The module stack was connected to a titanium stem (8 in Figure 1) which sealed against the quartz tube (1 in Figure 1). UV radiation was emitted by the LED modules and transmitted through the wall of the protective quartz tube.

A complete UV system was comprised of a stack of LED modules, a quartz tube, and a titanium stem (Figure 1, middle), with one complete system installed in each of the UV-equipped instruments (Figure 1, left). Each module stack was comprised of four LED modules: three modules with LEDs (UVTOP280TO39FW, 280 nm, Sensor Electronic Technology, Columbia, SC) oriented normal to the long axis of the UV system, referred to as sideways-facing modules (6 in Figure 1), and one module with an LED (UVCLEAN280TO39FW, 280 nm, Sensor Electronic Technology, Columbia, SC) facing 12^{o} off the long axis, located at the top of the stack distal to the titanium stem and referred to as an upward-facing module (5 in Figure 1). Each module could be individually oriented to enable UV emission in multiple directions simultaneously. The flat windows of the LEDs provided a wide beam spread, approximately 120^{o} in air, to maximize coverage. The sideways-facing modules were equipped with 0.5 mW (optical power at 30 mA operating current) LEDs, while the upward-facing modules were equipped with 1-3 mW LEDs (80 mA operating current). This was done to accommodate the difference in distances to the target surfaces: the upwards-facing modules provided protection to the conductivity sensors (2 in Figure 1) while the sideways-facing modules provided protection to the optical turbidity sensor (4 in Figure 1) and time-of-flight sound velocity sensor (3 in Figure 1), both of which had sensing surfaces closer to the UV system. To protect the sensing electrodes of the external field conductivity sensors, UV radiation is required to penetrate through the glass tubes of the sensor, necessitating the additional power of the 1-3 mW LEDs due to the attenuation of the glass. The sensing tubes of the conductivity sensor (2 in Figure 1) were made of fused quartz glass to facilitate UV transmission through the sensor, enabling irradiation of the electrodes housed within.

Located at the top of all sideways-facing modules was a PCB ring-contact board (10 in Figure 1) to make electrical connection with the two spring pins present on the bottom of all modules (9 in Figure 1), thus each module was electrically connected in parallel and operated in concert. The titanium stem was designed such that it would install into the "secondary-style" sensor port of the AML instrument, allowing it to sit proximal to the target sensing surfaces of the adjacent sensors as shown in Figure 1, left. Integrated into the stem was an indicator ring (7 in Figure 1) which illuminated red in concert with the LED modules to provide visual indication of UV emission.

One UV system was installed in each endcap of the two UV-protected instruments. For each UV system, the bottom two modules (indexed from the titanium stem upwards) were oriented to irradiate the sound velocity sensor, the third module was oriented to irradiate the top surface of the turbidity sensor, and the fourth module (upwards-facing) was oriented to irradiate the sensing tubes of the conductivity sensor. UV emission was effected in alternating periods of "on" and "off," referred to as a duty cycle. For this trial, a duty cycle of 50% was selected, consisting of ten minute "on" and "off" periods, respectively. Selection of this duty cycle was based on previous (unpublished) work by the authors that

suggested this was a conservative regiment suitable for a range of environments.

UV Numerical Light Model

It has been established that the performance of UV antifouling systems is dependent on fluence [Patil et al., 2007], defined as the fluence rate integrated over time on a given surface. To estimate fluence, the fluence rate must be known. However, the instrument's immersion in seawater and geometry of the sensor cluster make direct measurement of fluence rate impractical. Therefore, a numerical UV light model was developed.

In the UV system described, a ray begins with emission from a source LED, propagates through the air annulus surrounding the LED module, refracts at the air/quartz interface of the glass tube, transmits through the glass, refracts at the quartz/seawater interface, and finally propagates outward through the seawater towards the target surface. In the quartz and seawater media (and air to a lesser extent), the intensity (fluence rate) of a given light ray diminishes with propagation distance due to attenuation. This arises from two mechanisms: absorption of the radiation by the medium and scattering due to particles. This relationship is described by Beer-Lambert's Law [Preisendorfer, 1976]:

$$I = I_x e^{-(kx)}$$
$$k = \propto + \sigma \qquad (1)$$

Where I is fluence rate, I_x is initial fluence rate, x is the ray length. $\propto$ and σ are absorption and scattering coefficients for a given medium, respectively. Though there have been efforts to relate turbidity (scattering) to attenuation [Griffith and Halloran, 1997], work here has been done under the assumption of clear water. The attenuation coefficient and index of refraction for light emission at 280 nm in quartz glass is 0.45 /m and 1.5, respectively, as published in Kitamura et al. [2007]. The seawater attenuation values are 0.0353 /cm and 0.288 /cm, for absorption and scattering, respectively, given by Smith and Baker [1981]. The index of refraction of seawater at 20°C and 3.5% salinity (35.0 PSU) is approximately 1.37, as per Quan and Fry [1995].

At the intersection of two media (such as air and glass, or glass and seawater), rays are both reflected and refracted. The fluence rate of a refracted ray is a function of transmittance while the fluence rate of a reflected ray is a function of reflectance. This principle is described by the well-known Fresnel equations; however, it can be shown that Schlick's equations may be used in lieu [Schlick, 1998]:

$$R_0 = \left(\frac{n_1 - n_2}{n_1 + n_2}\right)^2$$

$$R = \begin{cases} R_0 + (1 - R_0)(1 - \cos\theta_i)^5, & n_1 \le n_2 \\ R_0 + (1 - R_0)(1 - \cos\theta_t)^5, & n_1 > n_2, \theta_i \le \theta_{crit} \\ 1, & n_1 > n_2,\ \theta_i > \theta_{crit} \end{cases}$$

$$T = 1 - R \qquad (2)$$

Where R and T are the reflectance and transmittance, θ_i and θ_t are angle of incidence and angle of refraction, respectively, calculated using Snell's law. θ_{crit} is the critical angle at which total internal reflection occurs, computed using:

$$\sin \theta_{crit} = \frac{n_1}{n_2} \quad (3)$$

Multiplying the incident fluence rate by the reflectance and transmittance yields the fluence rates of the reflected and transmitted rays, respectively:

$$I_{reflected} = I_{incident} R$$
$$I_{transmitted} = I_{incident} T \quad (4)$$

Thus using Equation 4, the resulting fluence rate of a given ray as it interacts with the two media interfaces may be computed. In the interest of simplicity, only transmitted rays are considered. As a given ray travels through each medium, its fluence rate as a function of distance may be computed using Equation 1. Therefore, using Equation 1 through Equation 4, the fluence rate and angle of a given ray may be computed as it travels from the source LED to the target surface.

UV emission from a given LED is not uniform with angle, measured from a reference angle normal to the optical window. Peak fluence rate (power ratio of 1) occurs at 0^o and reduces to approximately 50% (power ratio of 0.5) at 60^o, after which it precipitously diminishes. Data relating ray emission angle to power ratio is provided by the manufacturer. A custom script employing these equations was written in MATLAB (MathWorks Inc., Natick, MA). The code was used to produce a series of emissive rays at varying angles from the source LED, each with a fluence rate ratio as per the manufacturer's specifications. Each ray path was plotted according to the equations described and the fluence rate of each ray was computed along its length. The outputs of the script were emission and fluence rate plots, used to estimate fluence rates at various locations around the UV system.

LED emission power is a function of supplied voltage (or current). For this reason, the LED optical power parameter of the MATLAB code must be "tuned" to actual LED output at the provided voltage. To do this, fluence rate measurements were obtained using an optical power meter (918D-ST-UV, Newport Corporation, Irvine, CA) at various distances along the reference axis of both high power and low power LEDs (normal to LED face). The optical power parameter in the MATLAB code was then "tuned" such that fluence rate-distance measurements were in agreement with model predictions in air. The air-calibrated model was then used to estimate the fluence rates incident on sensing surfaces of the various sensors when deployed in seawater by producing a fluence rate contour map for each of the LED modules. On each contour map, a fluence rate value at a point approximating the location of the corresponding irradiated sensing surface (as measured from a 3D model of the instrument) was selected to yield fluence rate when in seawater. For example, the sensing surface of a turbidity sensor is the flat optical face, irradiated by the third sideways-facing LED module. A point corresponding to the centre of the optical face was selected on the appropriate contour plot to yield incident fluence rate while in seawater. This was repeated for all sensors.

Performance Assessment Criteria

Performances of the UV systems were qualitatively assessed by inspection of the equipment upon retrieval from the ocean. To

evaluate the performance of the UV systems in preserving measurement integrity, time series plots for each sensor type were produced. Time series data were down sampled by applying one-minute averages, then smoothed using "boxcar averaging" with a period of three hours.

To estimate absolute drift of both the experimental and reference conductivity sensors, physical water samples were collected near the test platform close to the end of the experimental deployment on the dates of June 23, 2014, and July 22, 2014. The salinities of the water samples were then determined using a laboratory salinometer (Laboratory AutoSal 8400B, Guildline Instruments Ltd., Smith Falls, ON) and "true" conductivity values were computed by back-calculating conductivity from the measured salinity using the UNESCO equations of state of seawater [Fofonoff and Millard, 1983]. The back-calculation was done using pressure and temperature measurements from the deployed instruments at the time of sample collection. Care was taken to ensure that all measurements were synchronous with the physical collection of the water samples.

Relative measurement drift between sensors was also assessed. This was done by synchronizing the data series for two given sensors of the same type and producing a set of measurement differences. Two sets of measurement differences were produced: one spanning the day of October 24, 2013, the first day of deployment, and a second spanning July 22, 2014, the last day of deployment. The median difference of each series was then tabulated and compared. This was repeated for all permutations of each sensor type.

RESULTS

UV Light Model

Through measurement of the optical power of multiple LEDs it was found that the average output powers of the low and high power LEDs were approximately 0.650 mW and 1.850 mW, respectively. The MATLAB model was "tuned" in accordance with these values and validated by comparing measured fluence rates at various distances against model estimates in air. As shown in Figure 2, agreement between measured values and model predictions were good.

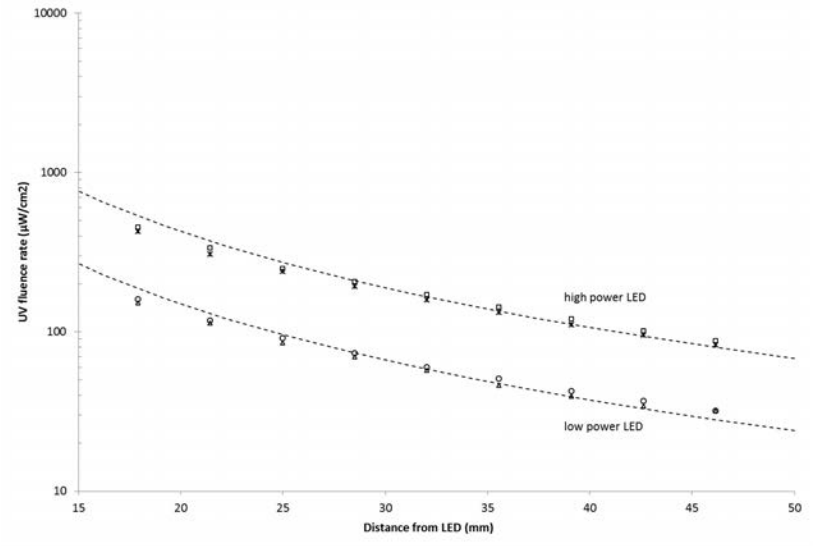

Figure 2: UV fluence rate versus distance from LED system in air. MATLAB model estimate shown as dashed line; measured values indicated as points.

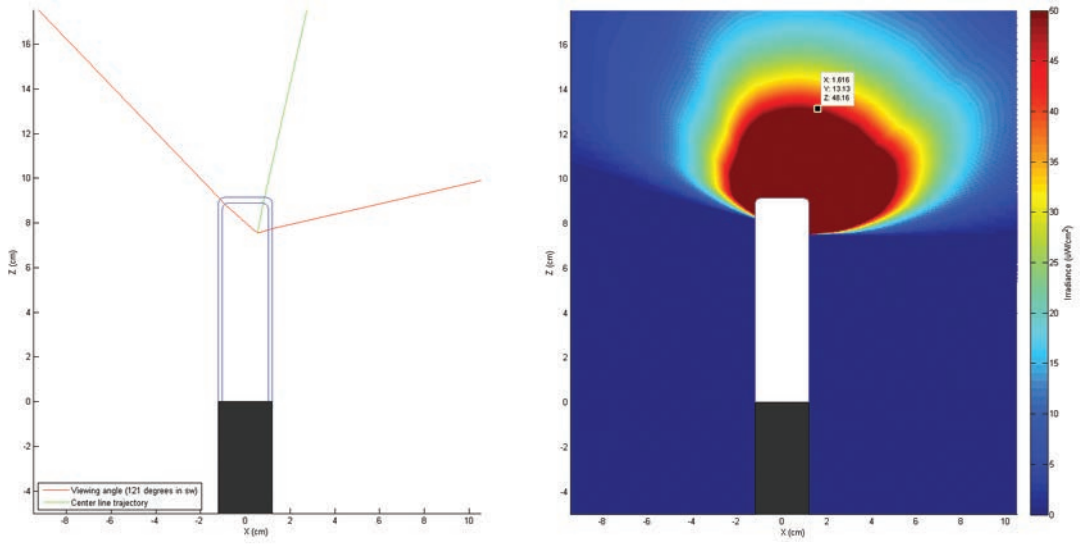

Figure 3: Left: Beam trajectory and limits of upwards-facing LED module in seawater. Right: UV fluence rate contour plot in seawater for upwards-facing LED module. Point indicates location of fluence rate measurement for conductivity sensor.

A fluence rate contour plot for an upwards-facing LED module is included in Figure 3 (right) – the module responsible for irradiating the conductivity sensors. As shown in the figure, the estimated fluence rate in seawater incident on the sensing tubes of the conductivity sensor is 48 μW/cm^2. At the duty cycle specified (ten minutes on/off), this yields a total UV fluence of 167 mJ/cm^2 each hour. The beam angle was calculated to be 121^o in seawater (Figure 3, left).

These results and the results for all remaining sensors are summarized in Table 1. The turbidity sensors were subject to the highest fluence rates, followed by the sound velocity sensors: 93 and 86 μW/cm^2, respectively.

Instrument Fouling Results

The two UV systems and sensors continued to operate for the duration of the deployment with a few notable events: 1) on January 11, 2014, a fragment of shell with live barnacles became lodged between the UV system and the turbidity sensor on instrument UV1, as shown in Figure 4 (middle); 2) on April 4, 2014, the upward-facing LED module on UV2 failed; and 3) on April 14, 2014, the sound velocity sensor failed on the control instrument.

When retrieved from the water at the end of the deployment, fouling on the instrument bodies and adjacent platform structures was extensive. The fouling was generally comprised of hard bodied organisms such as barnacles and was present on nearly all non-UV irradiated surfaces. During retrieval of the platform from the water, the shell fragment previously lodged in UV1 (refer to Figure 4) fell off. As shown in Figure 5, all UV-irradiated sensing surfaces were free of fouling, with the exception of the conductivity sensing tubes of instrument UV2, which exhibited minor soft-bodied fouling due to the LED module failure. The sensing elements of the protected turbidity sensors (1 in Figure 5), sound velocity sensors (2 in Figure 5), and the conductivity sensor of UV1 (4 in Figure 5)

Sensor	Location of measurement	Source of UV radiation	Fluence rate in seawater ($\mu W/cm^2$)	Fluence per hour (mJ/cm^2)
Turbidity	Centre of optical face	Module 3 (sideways facing)	93	167
Sound Velocity	Acoustic face	Modules 1 and 2 (sideways facing)	86	155
Conductivity	Top of sensing tubes (distal to instrument)	Module 4 (upwards facing)	48	86

Table 1: Estimated fluence rate and hourly fluence for UV-irradiated sensors.

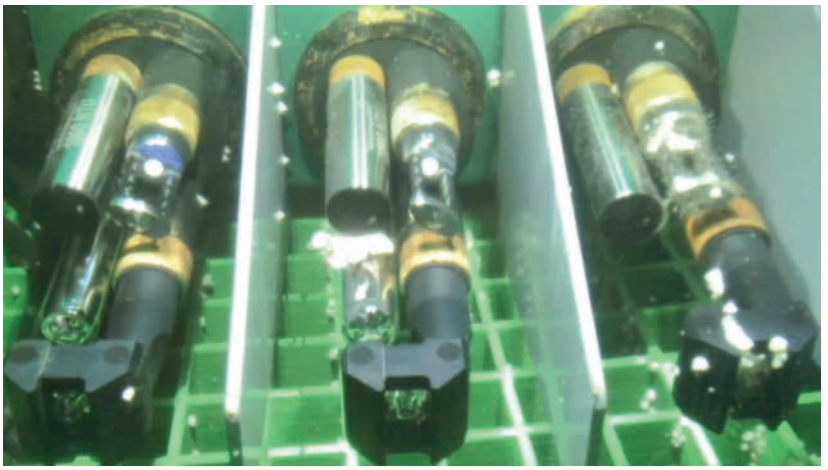

Figure 4: Test instruments in-situ. A shell fragment is lodged between the UV system and turbidity sensor on instrument UV1 (middle instrument). Fragment appeared suddenly on January 11, 2014.

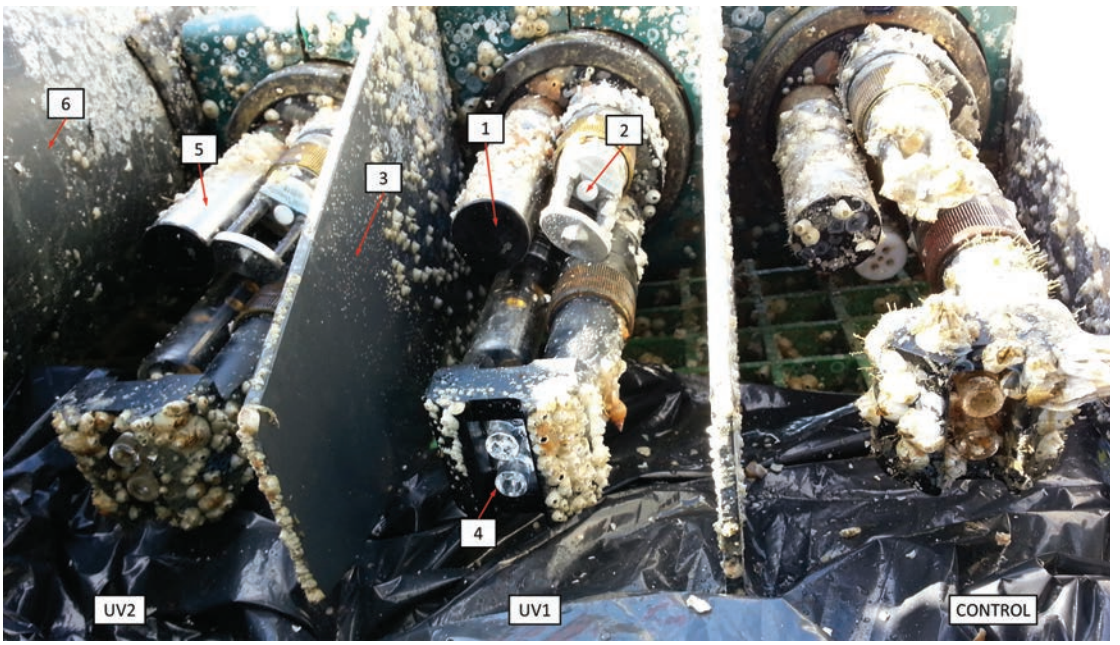

Figure 5: Test instruments post-deployment. UV-protected sensors have sensing surfaces devoid of fouling while control sensors are inundated. (1) sensing face of optical turbidity sensor, (2) sensing element of time-of-flight sound velocity sensor, (3) incidental fouling protection on adjacent structure, (4) completely clear sensing tubes of conductivity cell, (5) clear patches on body of turbidity sensor, (6) fouling-free area on adjacent structure. Image used with permission from Ocean Networks Canada Innovation Centre.

Figure 6: Camera sphere exhibiting signs of reduced fouling due to incidental UV exposure. UV test instruments located bottom right corner of image. Image used with permission from Ocean Networks Canada Innovation Centre.

were completely devoid of fouling. Additionally, adjacent surfaces were also observed to be free of fouling, indicated as (6 in Figure 5) and (3 in Figure 5), often with clear demarcations of the UV irradiation limits. The top (non-functional) surfaces of the UV-protected conductivity sensors exhibited fouling as they did not have line of sight with the UV systems.

As shown in Figure 6, the surface of the camera sphere facing the UV-protected instruments also exhibited a clear reduction in fouling. While not completely free of fouling, the UV-facing surface of the camera sphere was markedly cleaner than the remaining surfaces which did not have line of sight.

Sound Velocity Data

A plot of sound velocity measurements from the three sensors is included in Figure 7. As shown in the figure, the two UV-protected sensors (green and blue in the figure) were tracked for the duration of the deployment and are indistinguishable at the plot's scale. The control sensor (red) tracked the other two sensors for the first few months, then began to deviate around January and ultimately failed in April, approximately six months after deployment, presumably due to fouling (refer to Figure 5). The sensor on instrument UV2 (green) exhibited an increasing number of dropouts during the last one-and-a-half months of deployment.

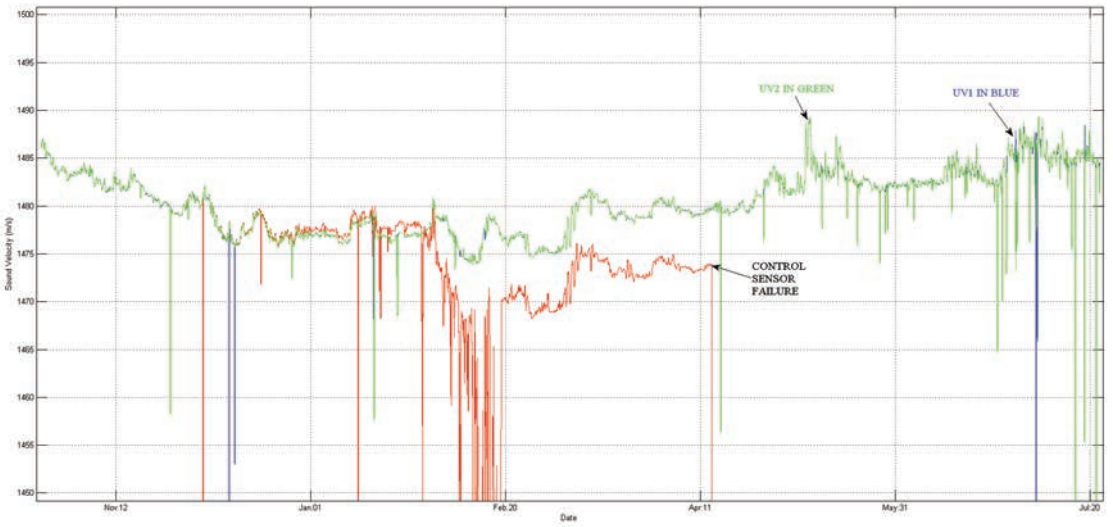

Figure 7: Sound velocity results. The control (unprotected) sensor failed on April 14, 2014.

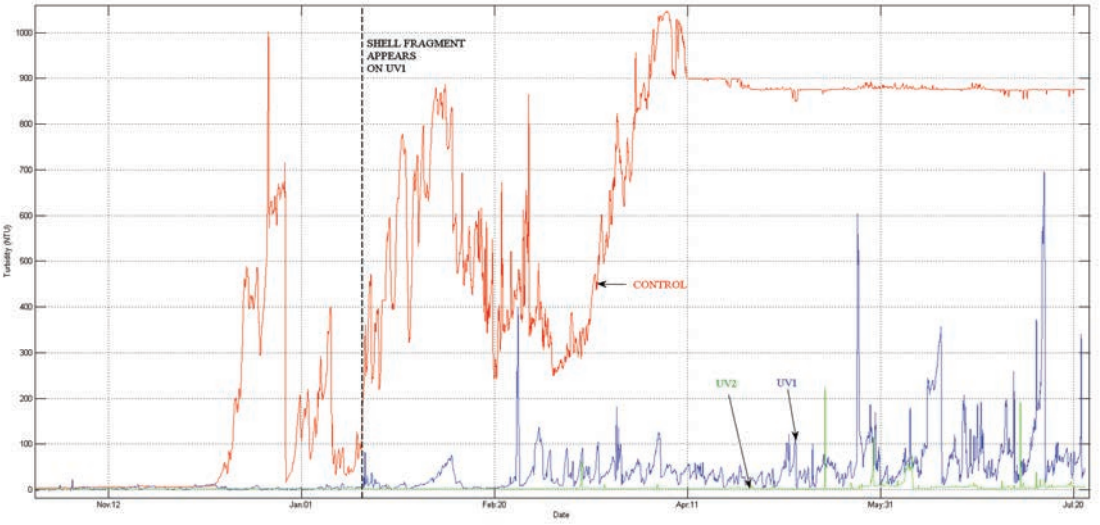

Figure 8: Turbidity sensor results. A shell fragment became lodged in the instrument UV1 on January 11, 2014.

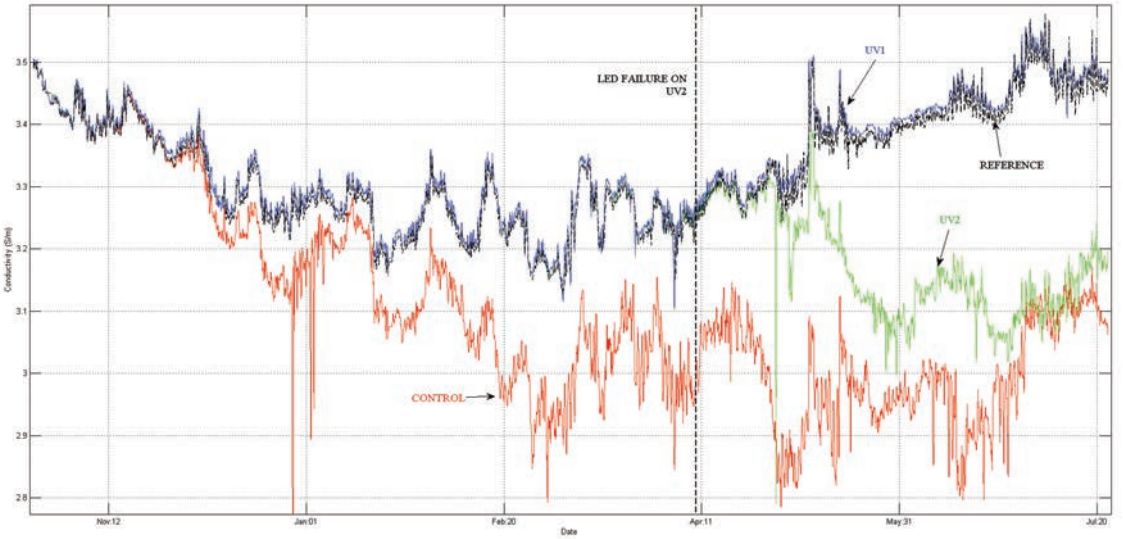

Figure 9: Conductivity results. LED failure on instrument UV2 occurred on April 4, 2014.

		Indicated Conductivity (mS/cm)	"True" conductivity (mS/cm)*	Difference (mS/cm)
June 23/14	**UV1**	34.183 +/- 0.010	34.143 +/- 0.002	0.040
	Reference Instrument	34.123 +/- 0.003	34.143 +/- 0.002	-0.020
July 22/14	**UV1**	34.814 +/- 0.010	34.902 +/- 0.002	-0.088
	Reference Instrument	34.831 +/- 0.003	34.902 +/- 0.002	-0.071

*Error estimate based on accuracy of salinometer (+/- 0.0001 conductivity ratio)

Table 2: Conductivity measurements vs "true" conductivity values.

Turbidity Data

Results from the turbidity sensors are included in Figure 8. The control instrument (red) demonstrated clear measurement deviation after two months, which increased with time. By seven months, the sensor stabilized around 900 NTU, just below its saturation point, likely due to hard-bodied fouling directly on the optical window. The turbidity sensors on instruments UV1 (blue) and UV2 (green) tracked each other until January 11, at which point the turbidity sensor on UV2 began to exhibit an increase in indicated turbidity. From this point on, turbidity indications from UV2 fluctuated between 0 and 200 NTU until the end of the deployment. In contrast, turbidity measurements from UV1 remained stable around 10 NTU.

Conductivity Data

Results from the conductivity sensors are included in Figure 9. After one-and-a-half months, the unprotected control sensor (red) began to measure values lower than the rest of the sensors with the offset increasing over time. In contrast, the two UV irradiated sensors closely tracked each other until early April, at which time the conductivity sensor on UV2 began to drift downwards, coinciding with the failure of the upwards-facing LED on that instrument. The reference conductivity sensor and the conductivity sensor on instrument UV1 tracked one another until the conclusion of the deployment, with a small offset (reference sensor reading lower).

Water samples were collected from the platform on June 23, 2014, and July 22, 2014. The "true" conductivity values were calculated to be 34.143 and 34.902 mS/cm, respectively. Neither the conductivity sensor on UV1 nor the reference sensors agreed with the "true" conductivity within error for either sample. In both instances, the magnitude of differences between measured and "true" conductivities for the reference sensor and the UV1 were comparable. These results are included in Table 2.

Progression of Measurement Differences

A summary of the median measurement differences between instrument series is included in Table 3. At the beginning of the deployment on October 24, 2013, measurements from all sound velocity sensors agreed within error. At the end of the

	Instruments Compared	Combined Sensor Accuracies (Max error)	Median Measurement Difference on Oct 24, 2013	Median Measurement Difference on July 22, 2014
Sound Velocity (m/s)	UV1-CONTROL	+/- 0.050	**0.042**	*Note 1*
	UV2-CONTROL	+/- 0.050	**0.016**	*Note 1*
	UV1-UV2	+/- 0.050	**0.028**	**0.017**
Turbidity (NTU)	UV1-CONTROL	+/- 1.0	5.3	836.0
	UV2-CONTROL	+/- 1.0	3.0	869.8
	UV1-UV2	+/- 1.0	2.3	33.6
Conductivity (mS/cm)	UV1-CONTROL	+/- 0.020	**0.005**	4.063
	UV2-CONTROL	+/- 0.020	**0.013**	1.120
	UV1-UV2	+/- 0.020	**0.008**	2.918
	UV1-REFERENCE	+/- 0.013	0.033	0.078
	UV2-REFERENCE	+/- 0.013	0.040	2.844

Table 3: Summary of measurement differences between instrument series.

Measurement differences within accuracy spec. indicated in bold
Note 1: Control sensor failed

deployment, measurements from sound velocity sensors on instruments UV1 and UV2 were still within error. A comparison against the control sound velocity sensor could not be made due to sensor failure.

Measurements from the turbidity sensors were not in agreement within error at the beginning of the deployment as the median differences were on the order of 5 NTU. By the end of the deployment, the control sensor differed from the two UV-protected sensors on the order of 800 NTU, indicating clear fouling of the control instrument, consistent with results shown in Figure 8. In contrast, the two UV-protected sensors differed by approximately 33 NTU at the conclusion of the deployment.

At the beginning of the deployment, all of the AML conductivity sensors agreed within error. None, however, agreed within error of the reference conductivity sensor. The two UV-protected sensors differed from the reference sensor by approximately 0.04 mS/cm. By the end of the deployment, the conductivity sensor of UV2 and the control sensor had fouled, resulting in large measurement errors; greater than 1 mS/cm. In contrast, the conductivity sensor on instrument UV1 differed from the reference sensor by 0.078 mS/cm, comparable to the beginning of the deployment.

DISCUSSION

Post-deployment inspection of the failed upward-facing LED module on UV1 has attributed the failure to a broken solder connection within the module. Function of the module was restored when the solder connection was repaired. The ultimate cause of the solder connection failure has not been determined.

It is evident from Figure 5 that the UV systems of instruments UV1 and UV2 were successful at eliminating fouling on all target surfaces. The sensing tubes of the conductivity sensor on instrument UV1 remained completely clear, comparable to when it was first deployed. Additionally, the antifouling influence of the UV systems is evident on the structures surrounding the UV-protected

instruments, even at unexpected distances. In particular, it is surprising to observe a clean patch on the camera sphere given its distance to the UV system (refer to Figure 6). The closest surface of the camera sphere is estimated to be approximately 50 cm from the test instruments. At this distance, the UV fluence rate is estimated to be on the order of 0.5 $\mu W/cm^2$, substantially lower than the energies used to protect the sensors. This suggests that there may be margin to decrease UV intensities incident on sensors while still maintaining antifouling performance. This also suggests that the UV system may be tolerant to a range of water turbidities as attenuation due to turbidity is moderate over the functional distances described here, and UV irradiation appears to be effective over a range of intensities. In general, every surface that had direct line of sight to a UV source and was within approximately 50 cm remained clear of fouling. This suggests that UV-C may be suitable for use as a general-purpose marine antifoulant, capable of protecting broad surface areas.

While the duration of the deployment described here extended for approximately nine months, all LEDs (with the exception of one) remained operational after retrieval, indicating that functionality of the UV systems would have endured had the deployment continued. The manufacturer of the LEDs specifies an L_{50} (time at which optical output diminishes to half of original power) of 5,000 hours – almost 14 months of continuous operation at the duty cycle described. This is likely an underestimate of ultimate functional lifetime as the LEDs will continue to operate past their L_{50}, with reduced power.

The results obtained from measurement series indicate that the UV systems were generally successful at preserving sensor measurement integrity. In regards to the sound velocity sensors, the two UV-protected sensors agreed within error after nine months of deployment (calculated difference of 0.017 m/s with an error budget of 0.050 m/S). While disagreement between UV-protected optical turbidity sensors increased over the deployment, this can be attributed to the barnacle shell that became wedged in the sensor cluster of UV1 rather than direct fouling of the sensor. This is substantiated by the fouling-free result of the sensor face shown in Figure 5 (middle). It is likely that the turbidity sensor was influenced by the continuously moving cirri of the live barnacles on the shell fragment lodged adjacent to it. This explanation is further supported through inspection of video footage: barnacle cirri movement was continuously occurring in close proximity to the optical face of the sensor, likely within its sensing volume. For these reasons, it can be stated that the UV systems successfully eliminated fouling induced measurement error of the two turbidity sensors. However, this result identifies a limitation of the technology: a UV-based antifoulant has no ability to remove debris that may either block UV irradiation or influence the sensor. The probability of such an occurrence may be reduced through the use of a protective cage over the sensor cluster, typical of most commercial sondes. Cages were not installed on these instruments to facilitate inspection via the remote camera.

The source of the occasional measurement dropouts on the sound velocity sensor of UV2

is not known for certain. The dropouts were not observed on the other UV-protected sound velocity sensor. It is possible that the dropouts may be attributed to interference from marine organism activity in the vicinity of the sensor. A review of camera footage revealed occasions of fish loitering in the vicinity of the sensor, as well as starfish and crabs. For reasons unclear, these occurrences were much more frequent on UV2 than UV1. It is also possible that the sensor was beginning to fail for reasons unrelated to fouling. Despite the occasional dropouts, measurements from the sound velocity sensor remained in agreement with the other UV-protected sensor.

The reference conductivity sensor described in this work uses a poison-based pumping system to control biofouling within the sensing volume of the internal field cell, considered the current industry standard. The median measurement difference between UV1 and the reference sensor from the beginning of the trial to the end of the trial are comparable: from 0.033 mS/cm at the beginning to 0.078 mS/cm at the end. Additionally, measurement error of the two sensors when compared with the "true" conductivity values for both water sample tests (refer to Table 1) were similar, with the reference sensor slightly closer to the "true" value in both instances. Together, these results suggest that the performance of the UV-based antifouling system was comparable to the poison-based system in reducing biofouling-induced measurement error in the conductivity sensors.

While effective in retarding biofouling, a limitation of this system is power consumption. At 80 mA and 30 mA for the high and low power LEDs, respectively (at 12 V), the current draw may be excessive for some power-sensitive deployments such as battery powered observatories or buoys. As UV-LED technology is currently nascent, it is anticipated that the efficiencies (and lifetimes) of the LEDs will improve in the future, reducing power consumption. Power savings may also be realized through additional strategies: while the expansive fouling-free surfaces in the vicinity of the UV systems demonstrate effectiveness, they also highlight that UV energy was spent on non-critical surfaces. To further reduce power consumption, more judicious use of UV energy is warranted. Shrouding the sensor group (and UV system embedded within it) with a protective cage that has a reflective inner surface will work to contain the UV energy in the vicinity of the sensing surfaces and allow secondary protection via reflective rays. This may further reduce the energy requirements of the system. Non-sensing surfaces may be protected through passive antifouling measures such as copper tape.

This work has not made an attempt to investigate the relationship between UV fluence rate and exposure time, nor to identify an optimal duty cycle. It has been suggested that exposure time is more important than fluence rate [Patil et al., 2007], possibly due to the repair mechanism inherent in cellular organisms to counteract the effect of UV damage. Additionally, minimizing UV "off time" may be important due to cellular division between times of UV exposure and the near-continuous adsorption of colonizing cells. The clean surface of the camera sphere (refer to Figure 6) may support this idea: the

UV fluence rate on the sphere was low, but the exposure time was comparatively large: 30 minutes of exposure per hour. As it is unclear if UV as an antifoulant exhibits time-fluence rate reciprocity [Lakretz et al., 2010; Patil et al., 2007], the optimal timing for UV emission remains to be determined. An additional factor is varying UV sensitivities among different organisms, suggesting that optimal duty cycles may be ecosystem-dependant. Future work is required to characterize these relationships with the goal of further reducing power consumption and increasing LED endurances.

CONCLUSION

This work established that UV-C radiation is effective at inhibiting marine biofouling on sensors and adjacent structures in long term in-situ deployments. Measurement integrity of the UV-protected sound velocity sensors was preserved. An increase in measurement disagreement between the two UV-protected optical turbidity sensors was attributed to the introduction of a shell fragment lodged between the sensor and UV system of instrument UV1. Inspection of the turbidity sensors post deployment revealed that the UV system was successful at keeping the sensing surfaces clear. Inspection of the UV-protected conductivity sensor also confirmed that the UV system was effective at eliminating growth within the sensor's sensing volume. Measurement disagreement between the reference conductivity sensor, protected by a chemical pumping system, and the conductivity sensor of instrument UV1 increased only slightly over the duration of the deployment, and water sample analysis revealed the errors of both sensors against the "true" conductivity were comparable. These results suggest that the efficacy of the UV system is comparable to the current industry standard in eliminating biofouling-induced measurement error.

Further work is required to characterize the parameters influencing UV performance. These parameters include duty cycle, fluence rate and its relationship to exposure time, and exposure mode. Understanding these parameters in conjunction with increases in UV-LED efficiency over time is expected to reduce the power requirements of the technology.

UV-C is an attractive antifoulant as it is non-contact, non-chemical and suitable for a broad spectrum of applications including protection of complex 3D surfaces and open-volumes. Extending the results of this investigation, UV may be suitable for protection of a wide range of underwater equipment including cameras, lights, ADCP acoustic faces, connectors, and various sensors.

ACKNOWLEDGMENT

The authors extend thanks to Ocean Networks Canada for its support in conducting this investigation.

REFERENCES

ACT Alliance for Coastal Technologies [2003]. *Biofouling prevention technologies for coastal sensors/sensor platforms*. UMCES Technical Report Series: TS-426-04-CBL, Solomons, Maryland.

Cooksey, K.E. and Wigglesworth-Cooksey, B. [1995]. *Adhesion of bacteria and diatoms to surfaces in the sea: a review*. Aquatic

Microbial Ecology, Vol. 9, No. 1, pp. 87-96.

Delauney, L.; Compere, C.; and Lehaitre, M. [2010]. *Biofouling protection for marine environmental sensors*. Ocean Science, Vol. 6, No. 2, pp. 503-511.

EPA Environmental Protection Agency [2003]. *UV disinfection guidance manual*. EPA 815-D-03-007.

Fofonoff, N.P. and Millard, R.C.J. [1983]. *Algorithms for computation of fundamental properties of seawater*. UNESCO Technical Papers in Marine Science, Vol. 51, p. 44.

Griffith, M.L. and Halloran, J.W. [1997]. *Scattering of ultraviolet radiation in turbid suspensions*. Journal of Applied Physics, Vol. 81, No. 6, p. 2538.

Hijnen, W.A.M.; Beerendonk, E.F.; and Medema, G.J. [2006]. *Inactivation credit of UV radiation for viruses, bacteria and protozoan (oo)cysts in water: a review*. Water Research, Vol. 40, No. 1, pp. 3-22.

Kitamura, R.; Pilon, L.; and Jonasz, M. [2007]. *Optical constants of silica glass from extreme ultraviolet to far infrared at near room temperature*. Applied Optics, Vol. 46, No. 33, p. 8118.

Kolappan, A. and Satheesh, S. [2011]. *Efficacy of UV treatment in the management of bacterial adhesion on hard surfaces*. Polish Journal of Microbiology, Vol. 60, No. 2, pp. 119-123.

Lakretz, A.; Ron, E.; and Mamane, H. [2010]. *Biofouling control in water by various UVC wavelengths and doses*. Biofouling, Vol. 26, No. 3, pp. 257-267.

Marconnet, C.; Houari, A.; Seyer, D.; Djafer, M.; Coriton, G.; Heim, V.; and Di Martino, P. [2011]. *Membrane biofouling control by UV irradiation*. Desalination, Vol. 276, No. 1-3, pp. 75-81.

Munshi, H.A.; Saeed, M.O.; Green, T.N.; Al-Hamza, A.A.; Farooque, M.A.; and Ismail, A.R.A. [2005]. *Impact of UV irradiation on controlling biofouling problems in NF-SWRO desalination process*. International Desalination Association World Congress Conference, Singapore.

Patil, J.S.; Kimoto, H.; Kimoto, T.; and Saino, T. [2007]. *Ultraviolet radiation (UV-C): a potential tool for the control of biofouling on marine optical instruments*. Biofouling, Vol. 23, No. 4, pp. 215-230.

Preisendorfer, R.W. [1976]. *Hydrologic Optics. Volume 2. Foundations*. U.S. Department of Commerce, National Oceanic and Atmospheric Administration, Environmental Research Laboratories, Pacific Marine Environmental Laboratory, Technical Report.

Quan, X. and Fry, E.S. [1995]. *Empirical equation for the index of refraction of seawater*. Applied Optics, Vol. 34, No. 18, p. 3477.

Rand, J.L.; Hofmann, R.; Alam, M.Z.B.; Chauret, C.; Cantwell, R.; Andrews, R.C.; and Gagnon, G.A. [2007]. *A field study evaluation for mitigating biofouling with chlorine dioxide or chlorine integrated with UV disinfection*. Water Research, Vol. 41, No. 9, pp. 1939-1948.

Schlick, C. [1998]. *An Inexpensive BRDF model for physically-based rendering*. Computer Graphics Forum, Vol. 13: pp. 233-246. doi: 10.1111/1467-8659.1330233.

Smith, R.C. and Baker, K.S. [1981]. *Optical properties of the clearest natural waters (200–800 nm)*. Applied Optics, Vol. 20, No. 2, p. 177.